AGU PUBLICATIONS

JGR

Journal of Geophysical Research: Solid Earth

RESEARCH ARTICLE
10.1002/2017JB015171

Key Points:
- We simulate the stick-slip dynamics in weakly wet, polydisperse granular fault gouge to illuminate underlying physics using 3-D DEM
- Longer slip recurrence times and higher stress drops are observed in wet fault gouge due to cohesive forces between wet particles
- Presence of liquid stabilizes shearing by increasing particle coordination number, enabling the system to make stronger force networks

Correspondence to:
O. Dorostkar,
domid@ethz.ch

Citation:
Dorostkar, O., Guyer, R. A., Johnson, P. A., Marone, C., & Carmeliet, J. (2018). Cohesion-induced stabilization in stick-slip dynamics of weakly wet, sheared granular fault gouge. *Journal of Geophysical Research: Solid Earth*, *123*, 2115–2126. https://doi.org/10.1002/2017JB015171

Received 31 OCT 2017
Accepted 22 FEB 2018
Accepted article online 28 FEB 2018
Published online 25 MAR 2018

Cohesion-Induced Stabilization in Stick-Slip Dynamics of Weakly Wet, Sheared Granular Fault Gouge

Omid Dorostkar[1,2,3], Robert A. Guyer[4,5], Paul A. Johnson[4], Chris Marone[6], and Jan Carmeliet[1,2]

[1]Chair of Building Physics, Department of Mechanical and Process Engineering, Swiss Federal Institute of Technology Zurich (ETH Zurich), Zurich, Switzerland, [2]Laboratory for Multiscale Studies in Building Physics, Swiss Federal Laboratories for Materials Science and Technology (Empa), Dübendorf, Switzerland, [3]Department of Civil, Environmental and Geomatic Engineering, Swiss Federal Institute of Technology Zurich (ETH Zurich), Zurich, Switzerland, [4]Solid Earth Geophysics Group, Los Alamos National Laboratory, Los Alamos, NM, USA, [5]Department of Physics, University of Nevada at Reno, Reno, NV, USA, [6]Department of Geosciences, Pennsylvania State University, University Park, PA, USA

Abstract We use three-dimensional discrete element calculations to study stick-slip dynamics in a weakly wet granular layer designed to simulate fault gouge. The granular gouge is constituted by 8,000 spherical particles with a polydisperse size distribution. At very low liquid content, liquids impose cohesive and viscous forces on particles. Our simulations show that by increasing the liquid content, friction increases and granular layer shows higher recurrence time between slip events. We also observe that slip events exhibit larger friction drop and layer compaction in wet system compared to dry. We demonstrate that a small volume of liquid induces cohesive forces between wet particles that are responsible for an increase in coordination number leading to a more stable arrangement of particles. This stabilization is evidenced with 2 orders of magnitude lower particle kinetic energy in wet system during stick phase. Similar to previous experimental studies, we observe enhanced frictional strength for wet granular layers. In experiments, the physicochemical processes are believed to be the main reason for such behavior; we show, however, that at low confining stresses, the hydromechanical effects of induced cohesion are sufficient for observed behavior. Our simulations illuminate the role of particle interactions and demonstrate the conditions under which induced cohesion plays a significant role in fault zone processes, including slip initiation, weakening, and failure.

1. Introduction

Fault gouge, the core of faults, generally contains granular materials created by wear, fragmentation, and comminution of surrounding wall rock (Collettini et al., 2009; Engelder, 1974; Marone, 1998; Marone et al., 1990; Shimamoto, 1979). The frictional properties of fault gouge and their evolution with shear govern key aspects of earthquake failure and the seismic cycle (Scholz, 1998; Scholz et al., 1972). In addition, the role of fluids is crucial in faulting physics, as shown from field work and highlighted in lab studies under a range of saturation states (De Paola et al., 2011; Mitchell & Faulkner, 2012; Scuderi et al., 2014, 2015; Scuderi & Collettini, 2016; Sibson, 1996) and numerical simulations (Dorostkar et al., 2017a, 2017b; Dorostkar, Johnson, et al., 2017).

Fluids influence mechanical and chemical aspects of faulting processes. Fluid-assisted mechanisms such as fault healing, pressure dissolution, and precipitation as well as hydrolytic weakening and fault lubrication dictate key aspects of fault mechanics. These processes have drastic influence on frictional properties of granular fault gouge and are able to change the characteristics of slip instabilities (Bos & Spiers, 2002; Niemeijer et al., 2008, 2010; Niemeijer & Spiers, 2006; Niemeijer et al., 2002; Pluymakers & Niemeijer, 2015; Renard et al., 2012; Scuderi et al., 2014; Tenthorey & Cox, 2006; Visser et al., 2012; Yasuhara et al., 2003, 2005; Zhang & Spiers, 2005; Zheng & Elsworth, 2013). Frictional properties are also found to be dependent on relative humidity and the mineral components in rock and other materials (Dieterich & Conrad, 1984; Frye & Marone, 2002). Frictional healing is recognized as combination of time-, displacement-, and velocity-dependent processes associated with fault restrengthening affecting the evolution of contact area at particle junctions (Chester, 1994; Dieterich & Kilgore, 1994; Ruina, 1983). For weakly wet granular gouge, Scuderi et al. (2014) found a systematic increase in maximum friction, frictional healing rate, and stick-slip friction drop by increasing relative humidity and that the evolution of contact area depends inversely on slip velocity and directly on relative humidity.

Numerical modeling is an asset for understanding the underlying physics of granular shear (e.g., Dorostkar & Mirghasemi, 2016; Dorostkar et al., 2017a, 2017b; Dorostkar, Johnson, et al., 2017; Kothari & Elbanna, 2017; Lieou et al., 2015; Pál et al., 2016). Moreover, numerical and analytical models provide a means to scale process-based models and laboratory results to tectonic scale. Numerical tools can provide grain scale information that helps to better understand the underlying physics of granular flow. One of the purposes of this paper is to explicitly investigate the mechanical rock interactions at the scale of grains within fault gouge. We compare dry and wet cases under identical conditions and analyze differences in terms of particle scale factors such as contact forces, capillary forces, coordination number, and other microscale parameters, in many cases building on our recent works (e.g., Dorostkar et al., 2017a, 2017b; Dorostkar, Johnson, et al., 2017).

In this paper, we study the hydromechanical effect of liquids on stick-slip dynamics in granular fault gouge. To simulate the presence of liquid at low saturation degree (pendular regime), in which isolated capillary bridges are formed between particles (Bocquet et al., 2002; Khamseh et al., 2015; Mitarai & Nori, 2006; Richefeu et al., 2007; Wang et al., 2017), we employ the capillary bridge model of *Soulié* (Soulié, Cherblanc, et al., 2006; Soulié, El Youssoufi, et al., 2006) that has been validated with experimental results (Gabrieli et al., 2012; Soulié, Cherblanc, et al., 2006; Soulié, El Youssoufi, et al., 2006). We also implement in our granular model viscous forces derived from lubrication theory (Goldman et al., 1967; Nase et al., 2001). We study the influence of capillary cohesion on the characteristics of slip instabilities including stick-slip recurrence time, stress drop, and fault layer compaction. We answer the question of "what are the effects of induced cohesion in weakly wet granular layer on stick-slip dynamics and how these effects scale with level of confining stress." We characterize these effects with particle scale metrics. We study conditions that include large shear displacements to gather sufficient stick-slip cycles for statistical analysis. Finally, we analyze how at grain scale the presence of liquid at low liquid contents can change the mechanical characteristics of contacts and how this is manifested in macroscale response. Although our focus in this study is on granular fault gouge, our observations can be inspirational for many geophysical phenomena including landslides and earth surface processes that involve granular physics.

2. Numerical Model

We use discrete element method (DEM) to model a granular layer representing a granular fault gouge. DEM was first introduced by Cundall and Strack to solve problems in rock mechanics (Cundall & Strack, 1979) and widely used in different fields in recent decades. The discrete nature of DEM enables grain scale analysis understanding the underling physics of phenomena especially for problems in geomechanics. In DEM, particles are tracked, and by considering the force balance, the equation of motion is solved for individual particles. The translational and angular equations of motion solved in DEM are presented as:

$$\sum F_{pi} = m_{pi}\left(\frac{d}{dt}u_{pi}\right), \tag{1}$$

$$\sum T_{pi} = I_{pi}\left(\frac{d}{dt}\omega_{pi}\right), \tag{2}$$

where m_{pi}, I_{pi}, u_{pi}, and ω_{pi} are mass, moment of inertia, and translational and angular velocities of particle i and F_{pi} and T_{pi} are forces and torques on particle i from particle-particle contacts, respectively. The particle-particle contact in DEM is modeled by combination of several rheological elements, that is, spring, dashpot, and slider, as is shown in Figure 1. In soft sphere DEM, overlap between particles is allowed and the normal and tangential contact forces are calculated as follows (Di Renzo & Di Maio, 2004):

$$F_{pn} = -k_{pn}\delta\varepsilon_{pn} + c_{pn}\delta u_{pn}, \tag{3}$$

$$F_{pt} = \min\left\{\left|k_{pt}\int_{t_{c,0}}^{t}\delta u_{pt}\,dt + c_{pt}\delta u_{pt}\right|, \mu_c F_{pn}\right\}, \tag{4}$$

where k_{pn} and k_{pt} are the normal and tangential spring stiffness, c_{pn} and c_{pt} are the normal and tangential damping coefficients, $\delta\varepsilon_{pn}$ is the overlap, δu_{pn} and δu_{pt} are the relative normal and tangential velocities of two particles in contact, and μ_c is the interparticle friction coefficient, respectively. The integral term in equation (4) shows an incremental spring that stores energy based on relative elastic tangential deformation of particle surface since the time when particles touched each other, $t_{c,0}$. If the Coulomb criterion is not met, the damping part in equation (4) is added to the tangential force component.

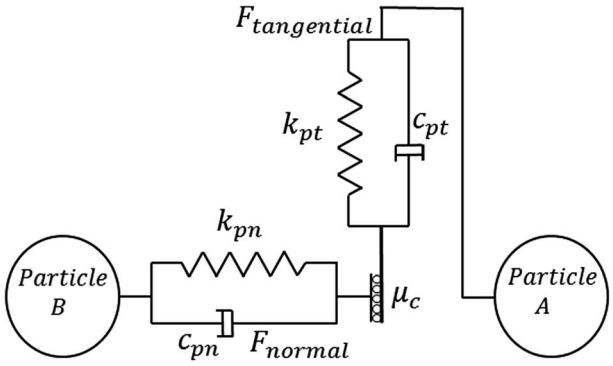

Figure 1. A schematic of structure of connected rheological elements representing a typical particle-particle contact model implemented in discrete element method algorithm. Elastic springs are denoted by k_{pn} and k_{pt} in normal and tangential directions, respectively. Contact dampers in normal and tangential directions are shown by dashpots, c_{pn} and c_{pt}, respectively. A slider denoted by μ_c controls the frictional limit according to the Coulomb friction law.

In order to capture particle scale nonlinearity, we use the nonlinear Hertzian contact law. In this particle-particle contact law, the spring stiffness and the coefficient of damping are function of particle material properties and the overlap between particles (Di Renzo & Di Maio, 2004; Hertz, 1882) and the normal and tangential contact forces are calculated as:

$$k_{pn} = \frac{4}{3} Y^* \sqrt{R^* \delta\varepsilon_{pn}}\,, \tag{5}$$

$$k_{pt} = 8\, G^* \sqrt{R^* \delta\varepsilon_{pn}}\,, \tag{6}$$

$$c_{pn} = -2\sqrt{\frac{5}{6}} \times \frac{\ln(r)}{\sqrt{\ln^2(r)+\pi^2}} \times \sqrt{2Y^* \sqrt{R^* \delta\varepsilon_{pn}} m^*}\,, \tag{7}$$

$$c_{pt} = -2\sqrt{\frac{5}{6}} \times \frac{\ln(r)}{\sqrt{\ln^2(r)+\pi^2}} \times \sqrt{8\, G^* \sqrt{R^* \delta\varepsilon_{pn}} m^*}\,, \tag{8}$$

where r is the restitution coefficient. In equations (5) to (8), Y^*, R^*, G^*, and m^* are the equivalent Young's modulus, radius, shear modulus, and mass for the two particles in contact, calculated as:

$$\frac{1}{Y^*} = \frac{(1-\upsilon_1^2)}{Y_1} + \frac{(1-\upsilon_2^2)}{Y_2}, \tag{9}$$

$$\frac{1}{G^*} = \frac{2(2-\nu_1)(1+\nu_1)}{Y_1} + \frac{2(2-\nu_2)(1+\nu_2)}{Y_2}, \tag{10}$$

$$\frac{1}{R^*} = \frac{1}{R_1} + \frac{1}{R_2}, \tag{11}$$

$$\frac{1}{m^*} = \frac{1}{m_1} + \frac{1}{m_2}, \tag{12}$$

where subscripts 1 and 2 denote the two particles in contact and υ is the poison ratio of particle.

We compare shear of dry granular particles with that of wet particles where a liquid film surrounds each particle and isolated capillary bridges may form between pairs of particles (Figure 2). For unsaturated cases and at low liquid content, capillary bridges may form between unequal size particles (R_1, R_2) with neck radius size of y_0 and interparticle distance of s (Figure 2c). The Laplace-Young equation describes the pressure difference of the capillary bridge (Soulié, El Youssoufi, et al., 2006):

$$\frac{\Delta p}{\sigma}\left(1+y'^2(x)\right)^{3/2} + \frac{1+y'^2(x)}{y(x)} - y''(x) = 0, \tag{13}$$

where $\Delta p = P_{gas} - P_{liquid}$ is the pressure difference across the gas-liquid interface, σ is the surface tension of liquid, and the y coordinate describes the liquid bridge profile across the x axis (Figure 2c).

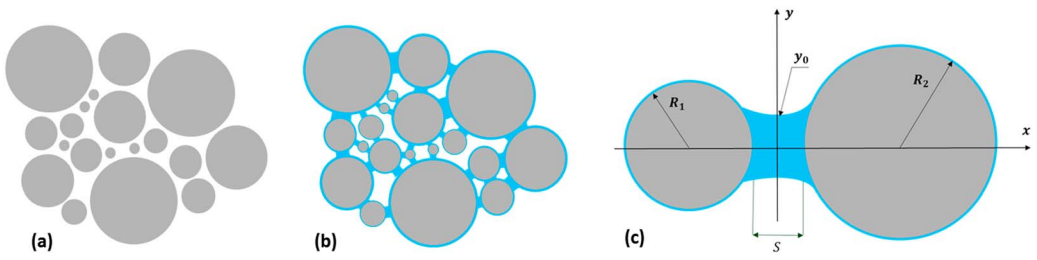

Figure 2. (a and b) The images show schematics of dry and wet granular particles. A liquid film is formed around each particle, and capillary bridges exist in the pendular state. (c) A capillary bridge with neck radius y_0 between two particles of radius R_1 and R_2 and a separation distance of s.

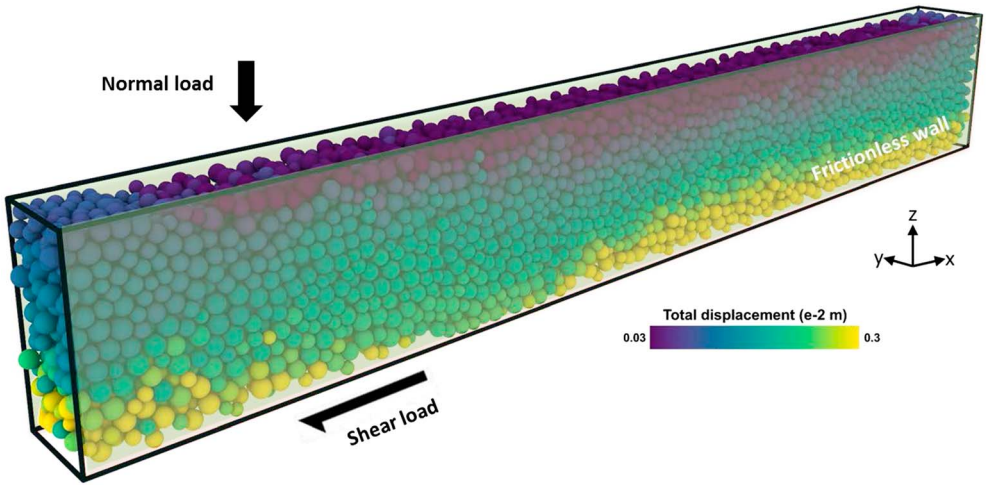

Figure 3. The granular fault gouge after the initial shear stage and before start of stick-slip dynamics. The color-coding shows total displacements (resultant of three components) of particles. The particle diameter ranges between 90 and 150 μm. A vertical load confines the layer (*z* direction) and remains constant during simulation. A displacement control mechanism is employed to shear the sample in *x* direction with constant velocity of 600 μm/s (image produced with the open source visualization tool OVITO; Stukowski, 2010).

The resultant force due to presence of liquid bridge consists of contributions from both the surface tension and the gas-liquid pressure difference and can be calculated at the gorge, for the neck radius of y_0 (Soulié, El Youssoufi, et al., 2006):

$$F = 2\pi y_0 \sigma + \pi {y_0}^2 \Delta p. \tag{14}$$

For DEM modeling, the capillary bridge force needs to be expressed explicitly as function of local geometrical and physical parameters (Soulié, El Youssoufi, et al., 2006). The equation describing this force is (Soulié, El Youssoufi, et al., 2006):

$$F = \pi\sigma\sqrt{R_1 R_2}\left[c + \exp\left(a + \frac{S}{R_{\max}} + b\right)\right], \tag{15}$$

where $R_{\max}$ is the larger radius of two particles in contact ($R_{\max} = \max\{R_1, R_2\}$) and S is the interparticle distance (Figure 2c), respectively. Coefficients a, b, and c are defined as:

$$a = -1.1\left(\frac{V}{R^3}\right)^{-0.53}, \tag{16}$$

$$b = \left(-0.148\ln\left(\frac{V}{R^3}\right) - 0.96\right)\theta^2 - 0.0082\ln\left(\frac{V}{R^3}\right) + 0.48, \tag{17}$$

$$c = 0.0018\ln\left(\frac{V}{R^3}\right) + 0.078. \tag{18}$$

In equations (16) to (18), V is the liquid bridge volume and θ is the contact angle, respectively. The bridge formation occurs upon contact of liquid films, and the rupture distance at which the bridges are broken is defined as proposed by Lian et al. (1993):

$$D_{\text{rupture}} = (1 + 0.5\theta)V^{1/3}, \tag{19}$$

where the volume of liquid bridge is calculated as $V = 0.05(V_i + V_j)$, in which V_i and V_j are the initial volume of liquid around each particle. In our simulations, the volume of liquid around each particle is initially defined and the bridge forms upon contact of two particles. The volume of liquid bridge will be evenly distributed between two particles after breakage of bridge, and the total volume of liquid in the sample will be

Table 1
Material and Simulation Properties

Property	Value	Property	Value
Sample size	11 * 1.5 * 0.8 mm	Confining stress	0.3–3 MPa
Particle density	2,900 kg/m^3	Shear velocity	600 μm/s
Particle diameter	90–150 μm	Time step	10^{-9} s
Particle Poisson ratio	0.25	Number of particles	8,000
Particle Young's modulus	65 GPa	Liquid surface tension	72 mN/s
Particle friction coefficient	0.5	Liquid-grain contact angle	0
Particle restitution coefficient	0.87	Liquid viscosity	10^{-3} Pa·s

constant (Soulié, El Youssoufi, et al., 2006). This model automatically instantiates a scalar transport equation that is solved for the surface liquid content of each particle, which is assumed to be small with no effect on the particle mass, diameter, and density (Kloss et al., 2012).

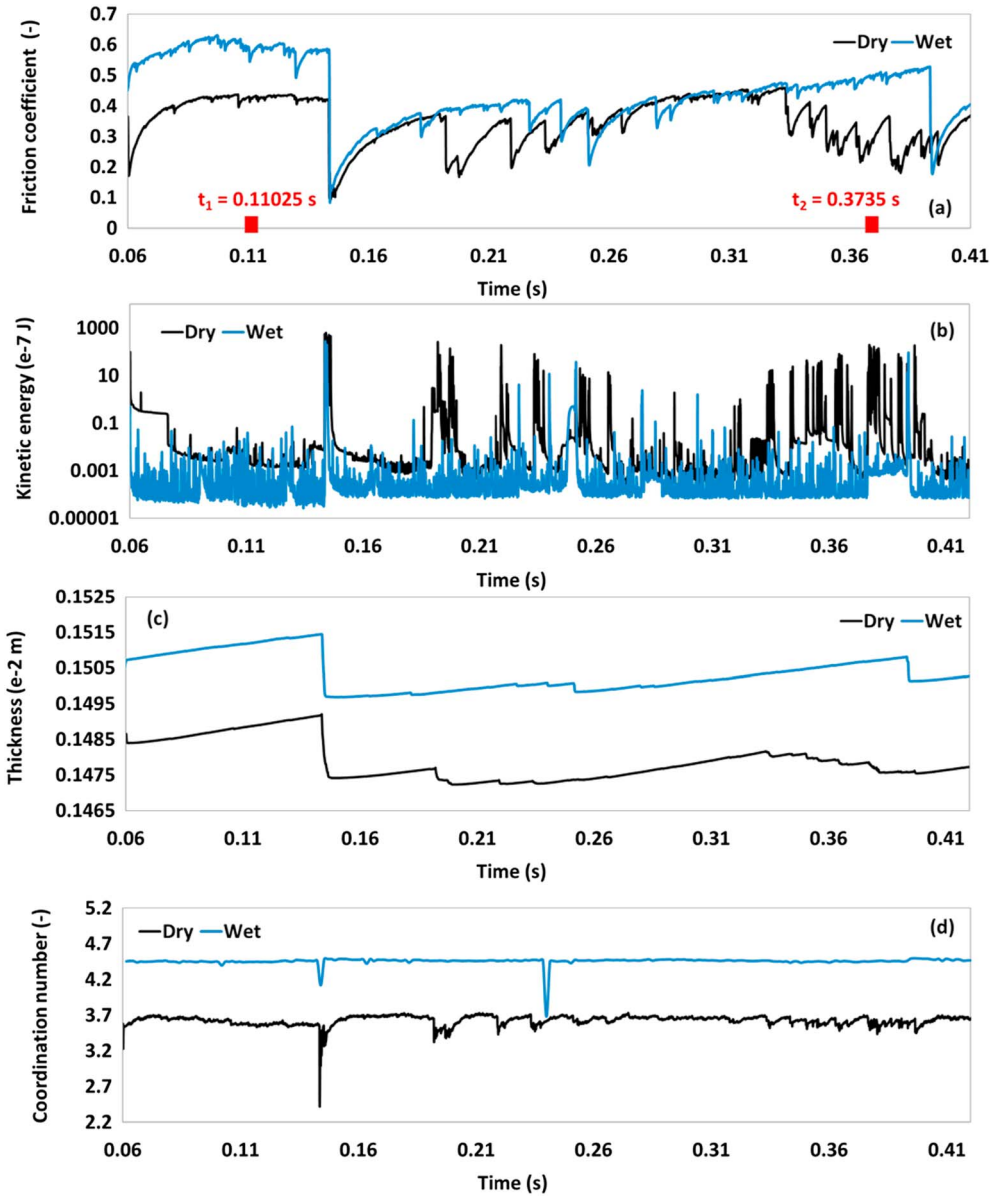

Figure 4. Representative runs of (a) friction coefficient, (b) kinetic energy, (c) layer thickness, and (d) average coordination number for dry and wet samples of 0.6% volumetric liquid content and confining stress of 300 kPa. The red squares in (a) show two points selected for contact force analysis in Figure 6.

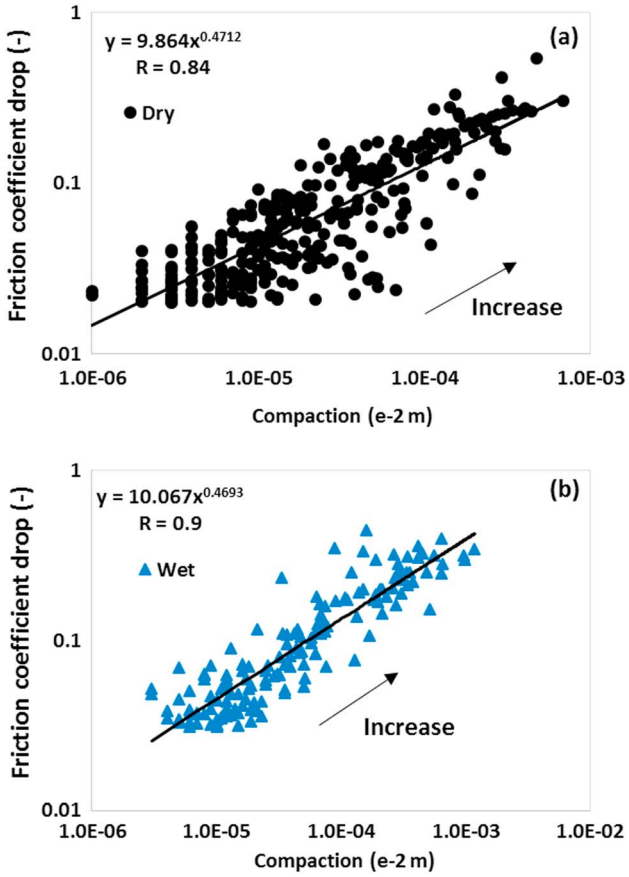

Figure 5. Log-log plot of friction coefficient drop versus granular layer compaction for (a) dry and (b) wet samples for large number of slip events.

Wet particles counter additional viscous forces that are resistant to their motion. These viscous forces are derived from lubrication theory (details of derivation can be found in Goldman et al. (1967)). The viscous forces acting on particles are (Nase et al., 2001):

$$F_{v_n=} 6\pi\mu R^* \vartheta_n \frac{R^*}{S}, \tag{20}$$

$$F_{v_t=} 6\pi\mu R^* \vartheta_t \left(\frac{8}{15}\ln\frac{R^*}{S} + 0.9588\right), \tag{21}$$

with

$$\frac{1}{R^*} = \frac{1}{R_1} + \frac{1}{R_2}, \tag{22}$$

where F_{v_n} and F_{v_t} are the normal and tangential viscous forces, ϑ_n and ϑ_t are the normal and tangential relative velocities of two particles in contact, μ is the liquid viscosity, and R^* is the equivalent radius, respectively. We use properties of water, that is, viscosity of 0.001 Pa·s and surface tension of 72 mN/m. The contact angle of water with the grain is assumed to be zero.

The granular layer contains 8,000 spherical particles that constitute the layer of simulated fault gouge (Figure 3). Periodic boundary conditions in the x direction allow for large displacements in the stick-slip regime, and as a result, many stick-slip cycles can be analyzed. As is shown in Figure 3, before the start of the stick-slip regime, the granular layer has undergone a large displacement where the entire granular sample is sheared. Frictionless walls in front and back are used avoiding rigid boundary conditions. Particles are generated randomly with a polydisperse particle size distribution ranging between 90 and 150 μm similar to the experiment (e.g., Scuderi et al., 2014).

The granular sample is confined under a constant confining stress of 0.3 or 3 MPa vertically (z direction in Figure 3) and sheared with a velocity of 0.6 mm/s horizontally (x direction in Figure 3). This loading configuration is chosen based on a phase-space study finding confining load and shear velocity range in which the granular layer undergoes stick-slip dynamics in a similar way to our recent works (Dorostkar et al., 2017a, 2017b).

The sample size is sufficiently large, $11 \times 1.5 \times 0.8$ mm^3, to have a proper 3-D force configuration (Ferdowsi, 2014; Dorostkar et al., 2017b). It is shown that the shear deformation in granular materials can localize in a shear band or span over the whole layer (Mühlhaus & Vardoulakis, 1987; Scuderi et al., 2017; Sulem et al., 2011). In our model, the simulated granular layer is considered as a part of the central shear layer in fault gouge, where the shear deformation spans over the whole layer thickness (see Figure 3). Granular particles have a density of 2,900 kg/m^3, Poisson's ratio of 0.25, Young's modulus of 65 GPa, particle friction coefficient of 0.5, and restitution coefficient of 0.87. These properties refer to glass beads as are used in the experimental analysis of Scuderi et al. (2014). Based on loading configuration and particle density, the DEM time step is set to 10^{-9} s leading to stable simulations in the quasi-static regime avoiding inertial effects. We limit the maximum volumetric liquid content to 1.8% to remain in the pendular regime (Mitarai & Nori, 2006). In pendular regime, the capillary bridges are isolated between pairs of particles. Simulation and material properties are summarized in Table 1. We use the open source software LIGGGHTS (Kloss et al., 2012) as our DEM solver.

3. Results

We document the evolution of bulk friction coefficient (defined as ratio of shear stress to confining stress), kinetic energy, and layer thickness for dry or wet samples with a range of volumetric liquid contents (Figure 4). The volumetric liquid content is defined as the ratio of the volume of liquid present in the sample to total volume of the sample. The kinetic energy consists of both rotational and translational kinetic energies. We find that a small amount of liquid causes higher average frictional strength and larger stick-slip

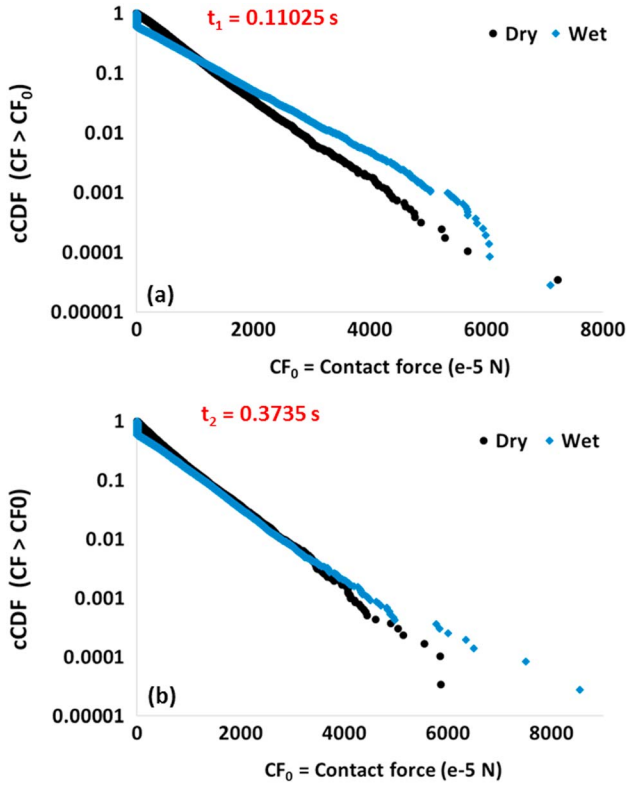

Figure 6. Complementary cumulative distribution function (cCDF) of contact forces for two points denoted in Figure 4a. In Figure 6, the volumetric liquid content is 0.6% and the confining stress is set to 300 kPa.

recurrence times. Figure 4a shows that for a wet granular layer, the friction coefficient (or shear stress) remains at higher levels for a longer time compared to dry condition. The values of kinetic energy in Figure 4b rapidly increase at slip and on average are lower for a wet compared to a dry sample. The granular layer stores potential energy during stick phase. The kinetic energy during this period is dominated by rotational kinetic energy (Dorostkar et al., 2017b). At slip, weakening happens and a portion of stored energy is converted to kinetic energy. Figure 4c shows that the granular layer dilates during the stick phase and compacts at slip. Previous studies have shown that the dilatational behavior can be attributed to rolling of particles while compaction is associated with a significant rearrangement (displacement) of particles (Dorostkar et al., 2017b). From Figure 4c, with the addition of liquid, the granular layer dilates more while being sheared, and the layer thickness is on average larger, which we will discuss in the following section.

We find that particle coordination number evolves systematically as a function of fluid content and shear (Figure 4). The coordination number is defined as the number of contacts per particle, which for the wet sample includes also those contacts without particle overlap but only with capillary bridges. We observe that the coordination number is almost constant during stick phase. At slip, the coordination number drops showing overall contact loss due to rearrangement of particles. The coordination number is on average higher for the wet sample. The higher coordination number indicates a stabilization of granular layer (Dorostkar et al., 2017a), as will be shown in more detail below.

The larger dilation (see Figure 4c) in wet sample is correlated with the larger macroscopic friction coefficient (Figure 4a), as also reported in experimental analysis (Scuderi et al., 2014). It is argued in the study of Scuderi et al. that the larger friction coefficient in wet samples promotes a dilatational behavior as manifested in thickness evolution (Scuderi et al., 2014). This interpretation will also be discussed below. Overall, our observations in Figure 4 show the important impact of the presence of a small volume of liquid on the mechanical behavior of the granular fault gouge changing characteristics of stick-slip dynamics.

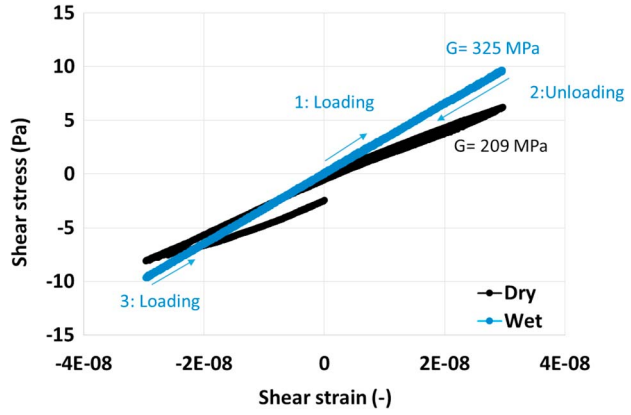

Figure 7. Shear stress-strain curves for dry and wet granular layers in a loading-unloading protocol during measurement of the shear modulus. The numbered blue arrows show loading-unloading steps. The slope of the first loading step is used to determine the shear modulus. The volumetric liquid content is 0.6%, and the confining stress is 300 kPa.

Our results show a clear correlation between stick-slip stress drop and corresponding layer compaction for both dry and wet samples (Figure 5). Slip instabilities cause particle rearrangement, and larger slips are accompanied by greater rearrangement of particles, leading to higher compaction, as reported in previous studies (Dorostkar et al., 2017b). For two points marked on the time axis of Figure 4a, we show in Figures 6a and 6b the distribution of contact forces for dry and wet simulations. The complementary cumulative distribution (cCDF) in Figure 6 is defined as:

$$\mathrm{cCDF}(Y < Y_0) = \mathrm{CDF}(Y > Y_0) = 1 - \mathrm{CDF}(Y < Y_0), \qquad (23)$$

where Y represents the contact forces. We see that distributions of contact forces in the wet sample start deviating from the dry curve around probabilities of 0.01. This observation implies that the strongest contacts in sample, with a total portion of around 1%, show larger contact forces in the wet sample. In the wet sample, the presence of small capillary/viscous forces between the particles leads to a more stable arrangement of particles characterized by a higher coordination number. This stable arrangement enables the granular

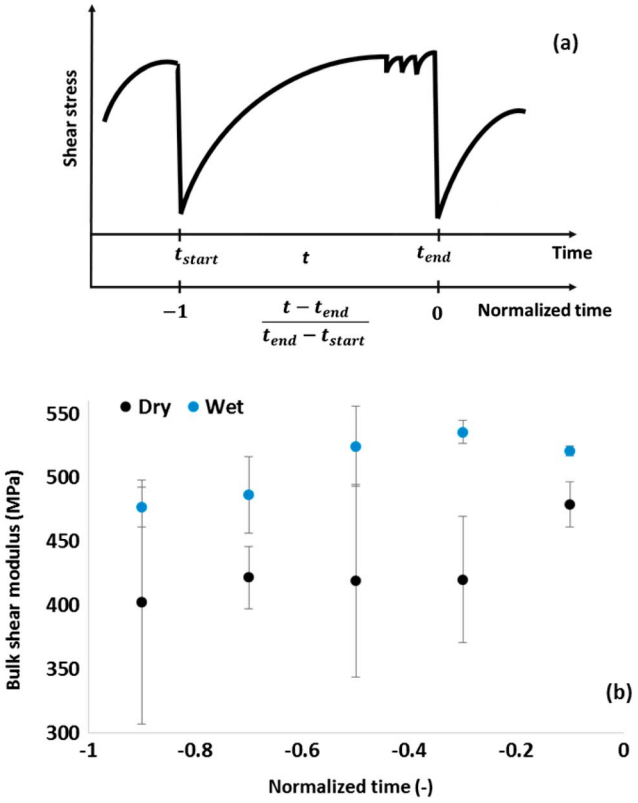

Figure 8. (a) Schematic stick-slip cycle with concept of normalized time. (b) Comparison of the shear modulus of dry and wet granular samples averaged over five different stick-slip cycles. The error bars indicate the standard deviation. The volumetric liquid content is 0.6%, and the confining stress is 300 kPa.

system to make some contacts stronger leading to a stabilization of the material. This stabilization is also clear from Figure 4b, where the kinetic energy of particles in wet sample during the stick phase is 2 orders of magnitude lower than in the dry system.

We hypothesize that such stabilization should be manifested also in an increase of the shear modulus of the granular system. In other words, when for a given shear strain, the wet granular layer shows a higher maximum shear stress, it is most likely that the shear modulus will be also higher. To test this hypothesis, we measure the bulk shear modulus of granular layer in dry and wet conditions. This measurement is performed using a loading/unloading protocol, as is shown in Figure 7. This figure shows an example of shear modulus measurements showing a higher value for the wet sample. To make sure that this finding is systematic and consistent for different stick-slip cycles, we select five stick-slip cycles for each system (dry and wet) and perform shear modulus measurements at different points during the stick phase. Since the stick-slip cycles have different time intervals, we normalize the time and divide the stick interval into five consecutive periods. The shear modulus measurements are averaged in each of these periods, as is shown in Figure 8. We observe on average a higher shear stiffness for wet samples, which confirms our hypothesis.

We further perform long simulations for three different levels of liquid content and determine the characteristics of the stick-slip cycles. To identify slip events, we use a threshold drop in friction larger than 0.03. This threshold is chosen by statistical analysis of long time series of friction coefficient signals, neglecting those small friction drops which can be attributed to small rearrangements of

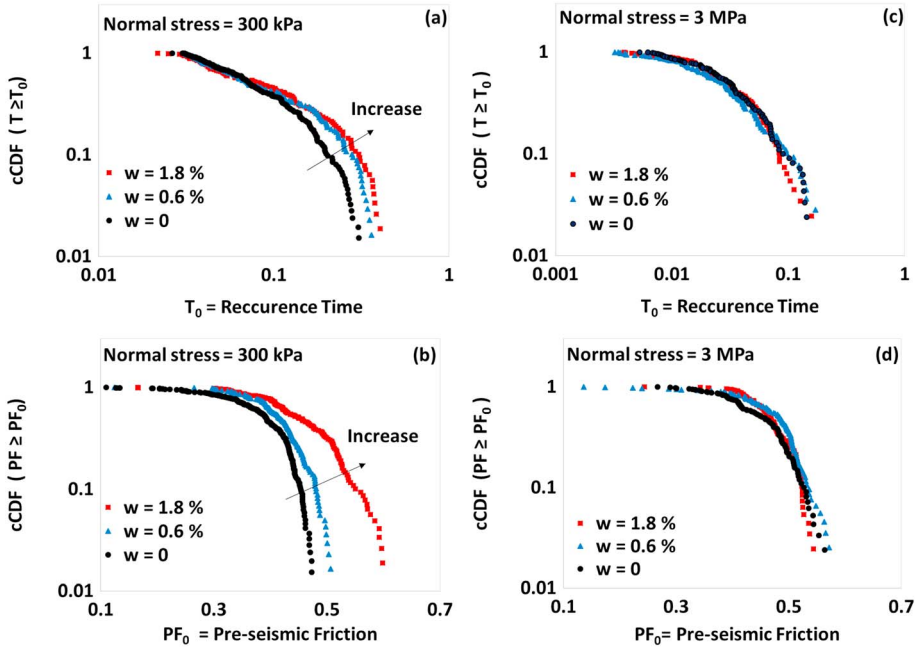

Figure 9. Complementary cumulative size distribution function of slip recurrence time and preseismic friction for simulations with confining stress of (a and b) 300 kPa and with confining stress of (c and d) 3 MPa, respectively.

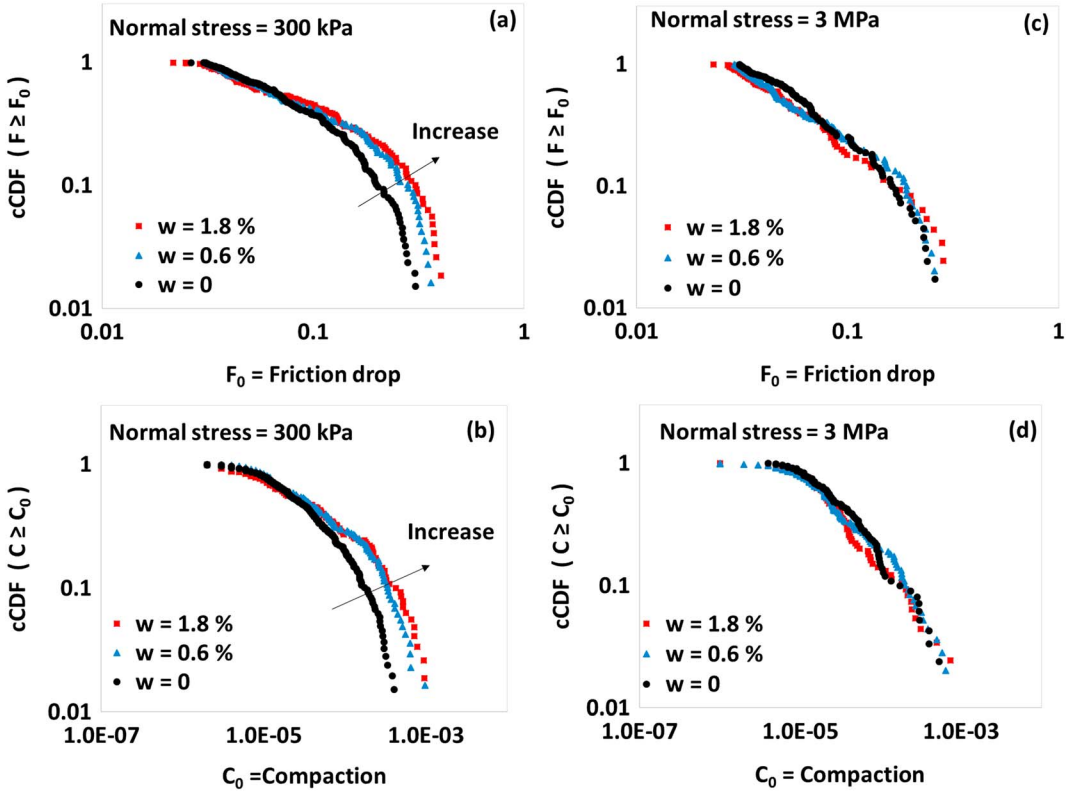

Figure 10. Complementary cumulative size distribution function of friction coefficient drop and compaction for simulations with confining stress of (a and b) 300 kPa and with confining stress of (c and d) 3 MPa, respectively.

particles, referred to as microslips (Ferdowsi et al., 2013), and to select only the major slip events. We conduct simulations for samples with volumetric liquid contents of 0% (dry), 0.6%, and 1.8%. We perform simulations at two different levels of confining stress, 300 kPa and 3 MPa. In Figure 9, we plot the cCDF of major slip events. The left column shows the results for 300 kPa confining stress (Figures 9a and 9b), while the right column shows results for 3 MPa (Figures 9c and 9d). Figure 9a shows that the recurrence time increases with volumetric liquid content. This means that in wet samples, the granular layer is stabilized for longer time before slip occurs.

In Figure 9b, we observe that the average preseismic friction coefficient (preseismic means immediately before slip events' onset) increases with liquid content. This increase in recurrence time and friction coefficient can be attributed to the stabilization of the layer due to the presence of capillary bridges, indicated by an increase in coordination number and shear modulus. However, we do not see an evident increase for slip recurrence time and preseismic friction coefficient for simulations with confining stress of 3 MPa (Figures 9c and 9d). Figures 10a and 10b also show the increase of friction coefficient drop and compaction (drop in thickness) for increase of liquid content, whereas the increase in characteristics of slip events is less evident for simulations at a confining stress of 3 MPa, as shown in Figures 10c and 10d. Indeed, at high confining stresses, capillary forces play a less important role to change the arrangement of granular system. The coordination number at low confining stress (300 kPa) increases on average 25%, while at high confining stress (3 MPa), it increases only by 15% for wet compared to dry system. Therefore, we observe that at high confining stress, particle arrangements are not sufficiently changed to alter the system's behavior substantially. In a complementary simulation, we decrease the liquid surface tension by a factor of 10 in order to evaluate the influence of capillary forces. Figure 11 shows representative runs of friction coefficient and average coordination number for dry and wet samples of 0.6% volumetric liquid content and confining stress of 300 kPa, where the wet simulation is conducted with a liquid surface tension of 7.2 mN/m. We observe that such a decrease of the liquid surface tension shows similar results to those applying an increase of the confining stress by the same factor (from 300 kPa to 3 MPa). In spite of a 15% increase in coordination number,

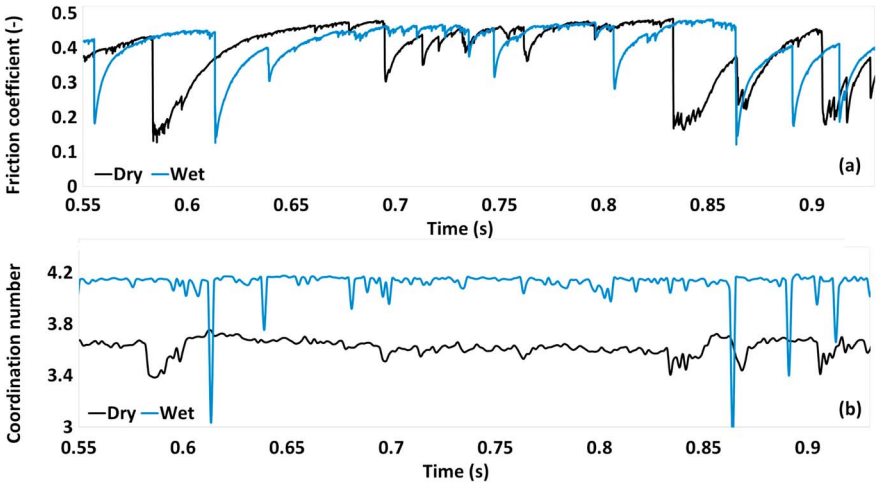

Figure 11. Representative runs of (a) friction coefficient and (b) average coordination number for dry and wet samples of 0.6% volumetric liquid content and confining stress of 300 kPa. The wet simulation is conducted with a liquid surface tension of 7.2 mN/m.

the evolution of friction coefficient is not significantly affected and the maximum friction coefficient is the same as for the dry sample.

We remark that our observations are consistent with experimental studies (Hornbaker et al., 1997; Louati et al., 2015; Richefeu et al., 2007; Scuderi et al., 2014). In experiments, Scuderi et al. (2014) observed that for wet samples, the preseismic friction coefficient and friction coefficient drop are higher compared to the dry condition. It has to be noted that our observations are achieved in the absence of chemical changes, alteration of asperities, and consequent change of interparticle friction coefficient in wet sample. The latter explanation was used in Scuderi et al. (2014) to explain their observations. Here in this paper we show that at low confining stresses, the presence of capillary bridges between the particles is sufficient to change the characteristics of stick-slip dynamics. As Hornbaker et al. (1997) mentioned, a small volume of liquid can dramatically change the properties of granular media, leading to a large increase in the repose angle, clustering, and correlation in grain motion. Our observations show, in both macro and grain scales, the importance of presence of small volumes of liquid on frictional strength and characteristics of slip instabilities in sheared granular layers.

4. Summary and Conclusions

We conducted 3-D DEM simulations to model slip instabilities in wet granular fault gouge. The wet particles are in the pendular regime with isolated capillary bridges imposing cohesive forces. Viscous forces resistant to particle motion that are derived from lubrication theory are also employed. Our results show that by increasing liquid content, the recurrence time of stick-slip events, the stress drop, and the average friction coefficient of slip events increase when applied loads are modest, in the range < 300 kPa. In addition, slip events involve greater particle rearrangement and greater layer compaction. Our grain scale observations show a more stable configuration for wet sample compared to dry, evidenced by higher coordination number and shear stiffness, which are consistent with macroscale phenomenological observations in our study as well as experimental investigations. We showed that the effect of capillarity on stick-slip dynamics disappears for higher stresses, above a few MPa. Our results show the importance of liquids and capillary forces for granular processes and highlight the versatility of numerical simulations using DEM.

Acknowledgments
The authors thank ETH Zurich for funding this study and Empa for infrastructural supports. Paul Johnson and Robert Guyer were funded by the institutional support (LDRD) at Los Alamos, as well as support from Empa. The data supporting this paper are available by contacting the corresponding author at domid@ethz.ch (Omid Dorostkar).

References

Bocquet, L., Charlaix, É., & Restagno, F. (2002). Physics of humid granular media. *Comptes Rendus Physique*, *3*(2), 207–215. https://doi.org/10.1016/S1631-0705(02)01312-9

Bos, B., & Spiers, C. J. (2002). Fluid-assisted healing processes in gouge-bearing faults: Insights from experiments on a rock analogue system. *Pure and Applied Geophysics*, *159*(11-12), 2537–2566. https://doi.org/10.1007/s00024-002-8747-2

Chester, F. M. (1994). Effects of temperature on friction: Constitutive equations and experiments with quartz gouge. *Journal of Geophysical Research*, *99*(B4), 7247–7261. https://doi.org/10.1029/93JB03110

Collettini, C., Niemeijer, A., Viti, C., & Marone, C. (2009). Fault zone fabric and fault weakness. *Nature*, *462*, 907. https://doi.org/10.1038/nature08585

Cundall, P. A., & Strack, O. D. (1979). A discrete numerical model for granular assemblies. *Géotechnique*, *29*(1), 47–65. https://doi.org/10.1680/geot.1979.29.1.47

De Paola, N., Hirose, T., Mitchell, T., Di Toro, G., Viti, C., & Shimamoto, T. (2011). Fault lubrication and earthquake propagation in thermally unstable rocks. *Geology*, *39*(1), 35–38. https://doi.org/10.1130/G31398.1

Di Renzo, A., & Di Maio, F. P. (2004). Comparison of contact-force models for the simulation of collisions in dem-based granular flow codes. *Chemical Engineering Science*, *59*(3), 525–541. https://doi.org/10.1016/j.ces.2003.09.037

Dieterich, J. H., & Conrad, G. (1984). Effect of humidity on time-dependent and velocity-dependent friction in rocks. *Journal of Geophysical Research*, *89*(NB6), 4196–4202. https://doi.org/10.1029/JB089iB06p04196

Dieterich, J. H., & Kilgore, B. D. (1994). Direct observation of frictional contacts: New insights for state-dependent properties. *Pure and Applied Geophysics*, *143*(1–3), 283–302. https://doi.org/10.1007/bf00874332

Dorostkar, O., Guyer, R. A., Johnson, P. A., Marone, C., & Carmeliet, J. (2017a). On the micromechanics of slip events in sheared, fluid saturated fault gouge. *Geophysical Research Letters*, *44*, 6101–6108. https://doi.org/10.1002/2017GL073768

Dorostkar, O., Guyer, R. A., Johnson, P. A., Marone, C., & Carmeliet, J. (2017b). On the role of fluids in stick-slip dynamics of saturated granular fault gouge using a coupled computational fluid dynamics-discrete element approach. *Journal of Geophysical Research: Solid Earth*, *122*, 3689–3700. https://doi.org/10.1002/2017JB014099

Dorostkar, O., Johnson, P., Guyer, R., Marone, C., & Carmeliet, J. (2017). Do fluids modify the stick-slip behavior of sheared granular media? In *Poromechanics VI: Proceedings of the Sixth Biot Conference on Poromechanics, 2017* (pp. 158–163). https://doi.org/10.1061/9780784480779.019

Dorostkar, O., & Mirghasemi, A. A. (2016). Micro-mechanical study of stress path and initial conditions in granular materials using dem. *Computational Mechanics*, *3*(1), 15–27. https://doi.org/10.1007/s40571-015-0074-3

Engelder, J. T. (1974). Cataclasis and the generation of fault gouge. *GSA Bulletin*, *85*(10), 1515–1522. https://doi.org/10.1130/0016-7606(1974)85%3C1515:CATGOF%3E2.0.CO;2

Ferdowsi, B. (2014). Discrete element modeling of triggered slip in faults with granular gouge: Application to dynamic earthquake triggering. (PhD dissertation), ETH Zurich.

Ferdowsi, B., Griffa, M., Guyer, R. A., Johnson, P. A., Marone, C., & Carmeliet, J. (2013). Microslips as precursors of large slip events in the stick-slip dynamics of sheared granular layers: A discrete element model analysis. *Geophysical Research Letters*, *40*, 4194–4198. https://doi.org/10.1002/grl.50813

Frye, K. M., & Marone, C. (2002). Effect of humidity on granular friction at room temperature. *Journal of Geophysical Research*, *107*(B11), 2309. https://doi.org/10.1029/2001JB000654

Gabrieli, F., Lambert, P., Cola, S., & Calvetti, F. (2012). Micromechanical modelling of erosion due to evaporation in a partially wet granular slope. *International Journal for Numerical and Analytical Methods in Geomechanics*, *36*(7), 918–943. https://doi.org/10.1002/nag.1038

Goldman, A. J., Cox, R. G., & Brenner, H. (1967). Slow viscous motion of a sphere parallel to a plane wall-i motion through a quiescent fluid. *Chemical Engineering Science*, *22*(4), 637–651. https://doi.org/10.1016/0009-2509(67)80047-2

Hertz, H. (1882). Ueber die berührung fester elastischer körper. *Journal fur die Reine und Angewandte Mathematik*, *92*, 156–171.

Hornbaker, D. J., Albert, R., Albert, I., Barabási, A. L., & Schiffer, P. (1997). What keeps sandcastles standing? *Nature*, *387*(6635), 765. https://doi.org/10.1038/42831

Khamseh, S., Roux, J.-N., & Chevoir, F. (2015). Flow of wet granular materials: A numerical study. *Physical Review E*, *92*(2), 022201.

Kloss, C., Goniva, C., Hager, A., Amberger, S., & Pirker, S. (2012). Models, algorithms and validation for opensource dem and cfd-dem. *Programming and Computer Fluid Dynamics*, *12*(2/3), 140–152. https://doi.org/10.1504/PCFD.2012.047457

Kothari, K. R., & Elbanna, A. E. (2017). Localization and instability in sheared granular materials: Role of friction and vibration. *Physical Review E*, *95*(2), 022901.

Lian, G., Thornton, C., & Adams, M. J. (1993). A theoretical study of the liquid bridge forces between two rigid spherical bodies. *Journal of Colloid and Interface Science*, *161*(1), 138–147. https://doi.org/10.1006/jcis.1993.1452

Lieou, C. K. C., Elbanna, A. E., Langer, J. S., & Carlson, J. M. (2015). Stick-slip instabilities in sheared granular flow: The role of friction and acoustic vibrations. *Physical Review E*, *92*(2), 022209.

Louati, H., Oulahna, D., & de Ryck, A. (2015). Apparent friction and cohesion of a partially wet granular material in steady-state shear. *Powder Technology*, *278*, 65–71. https://doi.org/10.1016/j.powtec.2015.03.011

Marone, C. (1998). Laboratory-derived friction laws and their application to seismic faulting. *Annual Review of Earth and Planetary Sciences*, *26*(1), 643–696. https://doi.org/10.1146/annurev.earth.26.1.643

Marone, C., Raleigh, C. B., & Scholz, C. H. (1990). Frictional behavior and constitutive modeling of simulated fault gouge. *Journal of Geophysical Research*, *95*(B5), 7007–7025. https://doi.org/10.1029/JB095iB05p07007

Mitarai, N., & Nori, F. (2006). Wet granular materials. *Advances in Physics*, *55*(1-2), 1–45. https://doi.org/10.1080/00018730600626065

Mitchell, T. M., & Faulkner, D. R. (2012). Towards quantifying the matrix permeability of fault damage zones in low porosity rocks. *Earth and Planetary Science Letters*, *339*, 24–31. https://doi.org/10.1016/j.epsl.2012.05.014

Mühlhaus, H. B., & Vardoulakis, I. (1987). The thickness of shear bands in granular materials. *Géotechnique*, *37*(3), 271–283. https://doi.org/10.1680/geot.1987.37.3.271

Nase, S. T., Vargas, W. L., Abatan, A. A., & McCarthy, J. J. (2001). Discrete characterization tools for cohesive granular material. *Powder Technology*, *116*(2–3), 214–223. https://doi.org/10.1016/S0032-5910(00)00398-3

Niemeijer, A. R., & Spiers, C. J. (2006). Velocity dependence of strength and healing behaviour in simulated phyllosilicate-bearing fault gouge. *Tectonophysics*, *427*(1–4), 231–253. https://doi.org/10.1016/j.tecto.2006.03.048

Niemeijer, A. R., Spiers, C. J., & Bos, B. (2002). Compaction creep of quartz sand at 400–600°c: Experimental evidence for dissolution-controlled pressure solution. *Earth and Planetary Science Letters*, *195*(3–4), 261–275. https://doi.org/10.1016/S0012-821X(01)00593-3

Niemeijer, A., Marone, C., & Elsworth, D. (2008). Healing of simulated fault gouges aided by pressure solution: Results from rock analogue experiments. *Journal of Geophysical Research*, *113*, B04204. https://doi.org/10.1029/2007JB005376

Niemeijer, A., Marone, C., & Elsworth, D. (2010). Frictional strength and strain weakening in simulated fault gouge: Competition between geometrical weakening and chemical strengthening. *Journal of Geophysical Research*, *115*, B10207. https://doi.org/10.1029/2009JB000838

Pál, G., Jánosi, Z., Kun, F., & Main, I. G. (2016). Fragmentation and shear band formation by slow compression of brittle porous media. *Physical Review E*, *94*(5), 053003.

Pluymakers, A. M. H., & Niemeijer, A. R. (2015). Healing and sliding stability of simulated anhydrite fault gouge: Effects of water, temperature and co_2. *Tectonophysics*, *656*, 111–130. https://doi.org/10.1016/j.tecto.2015.06.012

Renard, F., Beaupretre, S., Voisin, C., Zigone, D., Candela, T., Dysthe, D. K., & Gratier, J. P. (2012). Strength evolution of a reactive frictional interface is controlled by the dynamics of contacts and chemical effects. *Earth and Planetary Science Letters*, *341–344*, 20–34. https://doi.org/10.1016/j.epsl.2012.04.048

Richefeu, V., Youssoufi, M. S. E., & Radjaï, F. (2007). Shear strength of unsaturated soils: Experiments, dem simulations, and micromechanical analysis. In T. Schanz (Ed.), *Theoretical and numerical unsaturated soil mechanics* (pp. 83–91). Berlin, Heidelberg: Springer Berlin Heidelberg.

Ruina, A. (1983). Slip instability and state variable friction laws. *Journal of Geophysical Research*, *88*(B12), 10,359–10,370. https://doi.org/10.1029/JB088iB12p10359

Scholz, C. H. (1998). Earthquakes and friction laws. *Nature*, *391*(6662), 37–42. https://doi.org/10.1038/34097

Scholz, C., Molnar, P., & Johnson, T. (1972). Detailed studies of frictional sliding of granite and implications for the earthquake mechanism. *Journal of Geophysical Research*, *77*(32), 6392–6406. https://doi.org/10.1029/JB077i032p06392

Scuderi, M. M., & Collettini, C. (2016). The role of fluid pressure in induced vs. triggered seismicity: Insights from rock deformation experiments on carbonates. *Science Reporter UK*, *6*, 24852. https://doi.org/10.1038/srep24852

Scuderi, M. M., Carpenter, B. M., & Marone, C. (2014). Physicochemical processes of frictional healing: Effects of water on stick-slip stress drop and friction of granular fault gouge. *Journal of Geophysical Research: Solid Earth*, *119*, 4090–4105. https://doi.org/10.1002/2013jb010641

Scuderi, M. M., Carpenter, B. M., Johnson, P. A., & Marone, C. (2015). Poromechanics of stick-slip frictional sliding and strength recovery on tectonic faults. *Journal of Geophysical Research: Solid Earth*, *120*, 6895–6912. https://doi.org/10.1002/2015jb011983

Scuderi, M. M., Collettini, C., Viti, C., & E. T., & Marone, C. (2017). Evolution of shear fabric in granular fault gouge from stable sliding to stick slip and implications for fault slip mode. *Geology*, *45*(8), 731–734. https://doi.org/10.1130/G39033.1

Shimamoto, T. (1979). *Experimental studies of simulated gouge and their application to studies of natural fault zones*. Paper presented at the Conference VIII: Analysis of Actual Fault Zones in Bedrock, Natl. Earthquake Hazards Reduct. Program, Menlo Park, CA.

Sibson, R. H. (1996). Structural permeability of fluid-driven fault-fracture meshes. *Journal of Structural Geology*, *18*(8), 1031–1042. https://doi.org/10.1016/0191-8141(96)00032-6

Soulié, F., El Youssoufi, M. S., Cherblanc, F., & Saix, C. (2006). Capillary cohesion and mechanical strength of polydisperse granular materials. *The European Physical Journal E*, *21*(4), 349–357. https://doi.org/10.1140/epje/i2006-10076-2

Soulié, F., Cherblanc, F., El Youssoufi, M. S., & Saix, C. (2006). Influence of liquid bridges on the mechanical behaviour of polydisperse granular materials. *International Journal for Numerical and Analytical Methods in Geomechanics*, *30*(3), 213–228. https://doi.org/10.1002/nag.476

Stukowski, A. (2010). Visualization and analysis of atomistic simulation data with ovito—The open visualization tool. *Modelling and Simulation in Materials Science and Engineering*, *18*(1), 015012. https://doi.org/10.1088/0965-0393/18/1/015012

Sulem, J., Stefanou, I., & Veveakis, E. (2011). Stability analysis of undrained adiabatic shearing of a rock layer with cosserat microstructure. *Granular Matter*, *13*(3), 261–268. https://doi.org/10.1007/s10035-010-0244-1

Tenthorey, E., & Cox, S. F. (2006). Cohesive strengthening of fault zones during the interseismic period: An experimental study. *Journal of Geophysical Research*, *111*, B09202. https://doi.org/10.1029/2005JB004122

Visser, H. J. M., Spiers, C. J., & Hangx, S. J. T. (2012). Effects of interfacial energy on compaction creep by intergranular pressure solution: Theory versus experiments on a rock analog (nano3). *Journal of Geophysical Research*, *117*, B11211. https://doi.org/10.1029/2012JB009590

Wang, J.-P., Gallo, E., François, B., Gabrieli, F., & Lambert, P. (2017). Capillary force and rupture of funicular liquid bridges between three spherical bodies. *Powder Technology*, *305*, 89–98. https://doi.org/10.1016/j.powtec.2016.09.060

Yasuhara, H., Elsworth, D., & Polak, A. (2003). A mechanistic model for compaction of granular aggregates moderated by pressure solution. *Journal of Geophysical Research*, *108*(B11), 2530. https://doi.org/10.1029/2003JB002536

Yasuhara, H., Marone, C., & Elsworth, D. (2005). Fault zone restrengthening and frictional healing: The role of pressure solution. *Journal of Geophysical Research*, *110*, B06310. https://doi.org/10.1029/2004JB003327

Zhang, X., & Spiers, C. J. (2005). Compaction of granular calcite by pressure solution at room temperature and effects of pore fluid chemistry. *International Journal of Rock Mechanics and Mining Sciences*, *42*(7–8), 950–960. https://doi.org/10.1016/j.ijrmms.2005.05.017

Zheng, B., & Elsworth, D. (2013). Strength evolution in heterogeneous granular aggregates during chemo-mechanical compaction. *International Journal of Rock Mechanics and Mining Sciences*, *60*, 217–226. https://doi.org/10.1016/j.ijrmms.2012.12.031